Journal of Computational Physics 538 (2025) 114155

Contents lists available at ScienceDirect

Journal of Computational Physics

journal homepage: www.elsevier.com/locate/jcp

Casimir preserving numerical method for global multi-layer quasi-geostrophic turbulence

Arnout D. Franken [a,*], Erwin Luesink [a,b], Sagy R. Ephrati [c], Bernard J. Geurts [a,d]

[a] Multiscale Modelling and Simulation, Department of Applied Mathematics, Faculty EEMCS, University of Twente, PO Box 217, 7500 AE, Enschede, the Netherlands
[b] Now at Korteweg-de Vries Institute of Mathematics, University of Amsterdam, the Netherlands
[c] Department of Mathematical Sciences, Chalmers University of Technology, 412 96, Gothenburg, Sweden
[d] Multiscale Physics, Center for Computational Energy Research, Department of Applied Physics, Eindhoven University of Technology, Eindhoven, the Netherlands

ARTICLE INFO

Keywords:
Geostrophic turbulence
Geometric integrator
Lie–Poisson
Structure-preservation
Sphere

ABSTRACT

Accurate long-term predictions of large-scale flow features on planets are crucial for understanding global atmospheric and oceanic systems, necessitating the development of numerical methods that can preserve essential physical structures over extended simulation periods without excessive computational costs. Recent advancements in the study of global single-layer barotropic models have led to novel numerical methods based on Lie–Poisson discretization that preserve energy, enstrophy and higher-order moments of potential vorticity. This paper extends this approach to more complex stratified quasi-geostrophic (QG) systems on the sphere. These multi-layered models provide a more comprehensive representation of atmospheric and oceanic dynamics by accounting for vertical variations in density, pressure, and velocity fields.

In this work, we present a formulation of the multi-layer QG equations on the full globe. This allows for extending the Lie–Poisson discretization to multi-layer QG models, ensuring consistency with the underlying structure and enabling long-term simulations without additional regularization. The numerical method is benchmarked through simulations of forced geostrophic turbulence and the long-term behaviour of unforced multi-layered systems. These results demonstrate the structure-preserving properties and robustness of the proposed numerical method, paving the way for a better understanding of the role of high-order conserved quantities in large-scale geophysical flow dynamics.

1. Introduction

Long-time accurate predictions of large-scale flow features on planets are essential for understanding global climate systems [1]. These predictions underpin a range of applications, from weather forecasting to the study of climate change, and play a significant role in informing policy and strategic decisions aimed at addressing climate impacts.

A particular challenge in this field is the wide range of temporal and spatial scales involved in the full dynamic system. On the large planetary scales, an inverse energy cascade is present due to the two-dimensional nature of the flow at these scales, in which small eddies coalesce into increasingly larger eddies, thereby significantly contributing to the large-scale motion [2].

* Corresponding author.
E-mail address: arnoutfranken@live.nl (A.D. Franken).

https://doi.org/10.1016/j.jcp.2025.114155
Received 19 September 2024; Received in revised form 22 April 2025; Accepted 2 June 2025
Available online 4 June 2025
0021-9991/

The limitations of existing models primarily stem from the need to parameterize submesoscale processes due to computational constraints. Traditional approaches often involve additional modelling efforts to approximate the effects of these unresolved scales, leading to increased complexity and potential inaccuracies [3,4]. This underscores the importance of developing numerical methods capable of preserving essential physical structures over long simulation times without necessarily relying on such approximations.

The limitations of existing models often stem from numerical methods not reflecting the underlying basic dynamics, and the need to parameterize submesoscale processes due to computational constraints. Traditional approaches involve modelling efforts to approximate the effects of unresolved scales, leading to increased complexity and potential inaccuracies resulting from shortcomings in these submesoscale parameterizations. In some cases the submesoscale parameterization is adopted to contribute additional stability to the dynamical core of the model, but for the wrong reason, i.e., cloacking inherent instabilities in the numerical approach. In this paper, we create a structure-preserving, non-dissipative numerical method that is capable of preserving essential physical structures over long simulation times without the need to rely on approximations involving submesoscale parameterization. Conversely, with such computational model at hand, a sound basis is achieved to subsequently incorporate submesoscale parameterization to address physical challenges and not shortcomings in the numerical approach.

Structure-preserving (or geometric) numerical methods have been the subject of active research in recent years. These methods are designed to preserve numerically certain physical properties that arise naturally in conservative mechanics. Specifically, geometric methods boast excellent stability properties and produce statistically accurate results by restricting the solution space to be compatible with such physical constraints [5]. Traditional computational methods are generally unsuited for this purpose due to numerical truncation which causes errors to accumulate unphysically in long-time statistics.

Specifically, significant progress has recently been made through the development of structure-preserving numerical methods for single-layer barotropic models [6,7]. These methods exploit the Lie–Poisson structure of the governing equations, allowing for discretizations that inherently maintain the essential structure of the equations such as conservation laws. As a result, these methods enable long-term simulations without the need for additional regularization, providing a self-contained framework for modelling. The efficacy of these structure-preserving methods has been demonstrated in accurately capturing the energy spectra of two-dimensional turbulence [8], as well as capturing the essential large-scale dynamics of quasi-geostrophic flows [7].

Building on this foundation, the aim of this paper is to extend the applicability of structure-preserving numerical methods to more complex, multi-layer quasi-geostrophic models. Multi-layered models are crucial for a more comprehensive representation of atmospheric and oceanic dynamics, as they account for vertical variations in density, pressure, and velocity fields [9]. Extending these methods to multi-layer systems is a significant step towards capturing the intricate interactions between different layers of the atmosphere and ocean, as it extends the applicability of the models towards smaller scales.

In this paper, we present a detailed methodology for extending the structure-preserving Lie–Poisson discretization to multi-layer quasi-geostrophic models. The novelty of the current work is the combination of state-of-the-art numerical techniques that allow for efficient geometric integration of complex multi-layer quasi-geostrophic dynamics. Namely, our approach leverages the same principles as in the single-layer models by ensuring that the discretization remains consistent with the underlying physical structures. We demonstrate that these methods can accurately simulate the long-term behavior of multi-layer systems without requiring additional regularization. In doing so, we provide a benchmark for large-scale dynamics subject to external forcing and dissipation. Additionally, a unique property of the numerical method is the conservation of high-order moments of the potential vorticity (PV). Therefore, the numerical results demonstrate qualitatively how conserving these quantities impacts PV dynamics.

The structure of this paper is as follows. In Section 2, we derive the multi-layer QG equations on the sphere from the equations of motion without relying on tangent plane approximations. In this section, we highlight the influence of spherical geometry on the governing equations and introduce the Lie–Poisson formulation of the equation. Using this formulation, we derive a numerical model for these equations in Section 3 based on Zeitlin's method of quantisation. In Section 4, we show numerical results from two test cases, showing the structure-preserving properties of the numerical method. Conclusions and an outlook are given in Section 5.

2. Derivation of the global multi-layer QG equations

The multi-layer QG equation describes the evolution of potential vorticity (PV). Starting from the Primitive Equations (PE), the QG equations are typically derived on a local rectangular tangent plane to the sphere by taking a variational expansion around the geostrophic balance [9,10]. On this tangent plane, the Coriolis parameter is approximated as a constant or as a linear function of the latitudinal coordinate. This leads to the so-called f-plane and β-plane approximations respectively. The use of such a local domain implies the introduction of nonphysical boundary conditions. In this work, we will consider a global QG model, defined directly on the entire sphere. This enables the inclusion of the full Coriolis parameter, as well as the spherical geometry of the domain.

Previously, it was shown independently by Schubert et al. [11] and Verkley [12] that a global single-layer QG model can be derived from shallow water models by a solenoidal partitioning of the flow that distinguishes between a divergent and a non-divergent part. This provides an alternative to the traditional partitioning into a geostrophic and an ageostrophic component, which is ill-defined at the equator due to the vanishing Coriolis force. We follow the solenoidal partitioning of the flow and in this section derive the associated multi-layer QG model on the sphere. This multi-layer QG model on the sphere derived via the divergent/non-divergent splitting of the flow is new. This multi-layer model makes it possible to incorporate many essential phenomena that are not included in the single-layer QG model. Crucially, the single-layer QG model treats the fluid as a single homogeneous layer on top of a stationary surface. By including vertical variations in buoyancy, the multi-layer model includes internal baroclinic modes, which allows for the study of baroclinic instabilities [13,14].

The derivation of the multi-layer QG equations starts from the Boussinesq primitive equation (PE) (Section 2.1), to which an approximate quasi-geostrophic balance is imposed in case of stable stratification (Section 2.2), from which a multi-layer model can be derived (Section 2.4).

2.1. Boussinesq primitive equations on the sphere

The stratified QG equations can be derived from the Boussinesq PE, which describes the motion of a stratified hydrostatic fluid layer. A comprehensive derivation from Newton's equation of motion is provided in Pedlosky [10] and Vallis [9] on a tangent plane of the sphere. In this section, we use this approach to similarly derive the Boussinesq PE on a spherical domain from which the stratified QG equations can then be derived.

We consider a shallow layer of incompressible fluid on a sphere of radius R rotating with angular velocity $\mathbf{\Omega}$ obeying Newton's equation of motion. The assumption of a perfect sphere upon which a fluid layer is deposited that is very shallow compared to the radius of the sphere, yields by good approximation a uniform and constant gravitational acceleration $-g$ in the radial direction [15]. On a tangent plane the centrifugal force due to rotation counterbalances the gravitational acceleration, and only the Coriolis force appears in the equations of motion. The equations describing a Boussinesq fluid are subjected to two further basic assumptions that are adopted with respect to large-scale planetary flow:

1. in planetary flows, vertical velocity is small compared to horizontal velocities
2. inertial accelerations are very small compared to gravitational acceleration

As a result of these assumptions, large-scale motion in the radial momentum equation is close to hydrostatic equilibrium. The primitive equations (PE) in the Boussinesq approximation on the sphere with coordinates (r, ϕ, θ) are given by

$$\frac{\partial \mathbf{v}_h}{\partial t} + \mathbf{v} \cdot \nabla \mathbf{v}_h + f \hat{\mathbf{r}} \times \mathbf{v}_h = -\frac{1}{\rho_0} \nabla_h p, \tag{1}$$

$$\frac{\partial p}{\partial r} + \rho' g = 0, \tag{2}$$

$$\frac{\partial \rho'}{\partial t} + \mathbf{v} \cdot \nabla \rho' + w \frac{\partial \overline{\rho}}{\partial r} = 0, \tag{3}$$

$$\nabla_h \cdot \mathbf{v}_h + \frac{1}{r^2} \frac{\partial r^2 w}{\partial r} = 0, \tag{4}$$

where $\mathbf{v}_h$ is the tangential velocity field, w is the radial velocity, p is the pressure, ρ' represents fluctuations in buoyancy, ρ_0 is a constant, and $f = 2\Omega \cos \phi$ is the Coriolis parameter with Ω the magnitude of the angular velocity vector. The first two equations follow from the tangential (horizontal) and radial momentum equations respectively, the third equation describes transport of density fluctuations that follow from buoyancy and the fourth equation is the incompressibility condition. Together, they form the familiar Boussinesq PE on the sphere [16]. A conserved potential vorticity variable can be derived from these equations, see [17]. In the case of a stably stratified fluid, the equations can be reformulated in isopycnal coordinates, where the conserved potential vorticity is Ertel's potential vorticity, see [18] for more details. The buoyancy fluctuations are typically due to fluctuations in temperature, in which case one can explicitly write $\rho' = -\rho_0 \alpha T$, where T is the temperature and α is the thermal expansion coefficient. Other reasons for buoyancy fluctuations include changes in salinity. For generality, we therefore continue the analysis with ρ'.

Eqs. (1)–(4) are in their dimensional form and pertain to shallow water conditions. Specifically, Eq. (4) appears as a model for the deep atmosphere. However, upon introducing the aspect ratio of radial length scale compared to tangential length scale, as resulting from a non-dimensionalization, the incompressibility condition (4) will also take on its familiar form for shallow fluids.

The velocity vector $\mathbf{v}$ is split into its radial component w and the horizontal velocity field $\mathbf{v}_h$, given by $\mathbf{v} = \mathbf{v}_h + w\hat{\mathbf{r}}$, such that $\mathbf{v}_h \cdot \hat{\mathbf{r}} = 0$. To highlight this decomposition further, we write the del operator as ∇_h in case all radial derivatives are zero. Typically, the average density stratification is given which implies that these equations provide a closed system in terms of the velocity field and the fluctuating parts of density and pressure. In the next subsection, we use scaling arguments to derive the stratified QG equations on the sphere.

2.2. Stratified quasi-geostrophic equations on the sphere

The PE as formulated above constitute a complex model of the dynamics of a shallow fluid layer on a rapidly rotating planet. In the study of large-scale motions of this fluid, it appears that a large separation exists in the magnitude of the independent variables in the equations. To examine this, we consider scaling these equations and selecting a length scale for the horizontal motion L, as well as a horizontal velocity scale U. The length scale for vertical motion is the mean height of the fluid column, denoted by H, for which a vertical velocity scale W can be determined as $W = UH/L$. Since we are mainly interested in the horizontal motion, we introduce a time scale $T \sim L/U$. For the rotation of the sphere, the scale is given by Ω, while the density scale has already been given as ρ_0. We now assume that the parameters are such that the so-called global Rossby number is small, i.e., $\mathrm{Ro} = U/L\Omega \ll 1$, which holds for sufficiently large-scale horizontal motion. This is the core assumption for geostrophic flow, which implies that inertial forces are small compared to the Coriolis and gravitational forces [13], which implies a balance between the latter two forces, such that the momentum Eq. (1) yields

$$\left| f \hat{\mathbf{r}} \times \mathbf{v}_h \right| \sim \left| \frac{1}{\rho_0} \nabla_h p' \right|. \tag{5}$$

It is important to note that this does not hold in a small equatorial region on the sphere where f goes to zero. In other words, the motion in that region is not strictly geostrophic. Away from the equator, this balance is however quite accurate, which leads to a natural scaling of $p' \sim \rho_0 \Omega U L$. The hydrostatic balance (**??**) then yields the scaling of density fluctuations $\rho' \sim \rho_0 \Omega U L / gH$.

Finally, as is customary for stratified Boussinesq flows, we rewrite the average vertical density stratification by the Brunt-Väisälä frequency N, defined as

$$N(r) = \sqrt{-\frac{g}{\rho_0}\frac{\partial \rho'}{\partial r}}, \tag{6}$$

which represents the oscillating frequency of a displaced fluid parcel in a density gradient. This allows us to write the continuity Eq. (3) as

$$\frac{\partial \rho'}{\partial t} + \mathbf{v} \cdot \nabla \rho' - \frac{\rho_0}{g} w N^2 = 0. \tag{7}$$

Including a typical Brunt–Väisälä frequency N_0 leads to the following scalings,

$$\begin{aligned} &\mathbf{v}_h = \tilde{\mathbf{v}}_h U, \quad && w = \tilde{w}\tfrac{UH}{L}, \quad && t = \tilde{t}\tfrac{L}{U}, \quad && f = \tilde{f}\Omega \\ &N = \tilde{N} N_0, \quad && p' = \tilde{p}' \rho_0 g H, \quad && \rho' = \tilde{\rho}' \rho_0. && \end{aligned}$$

We non-dimensionalise the PE in terms of non-dimensionalised variables denoted with a $\sim$ as

$$\mathrm{Ro}\left(\frac{\partial \tilde{\mathbf{v}}_h}{\partial \tilde{t}} + \tilde{\mathbf{v}} \cdot \tilde{\nabla}\tilde{\mathbf{v}}_h\right) + \tilde{f}\hat{\mathbf{r}} \times \tilde{\mathbf{v}}_h = -\tilde{\nabla}_h \tilde{p}', \tag{8}$$

$$\frac{\partial \tilde{p}'}{\partial \tilde{r}} + \tilde{\rho}' = 0, \tag{9}$$

$$\mathrm{Ro}\left(\frac{\partial \tilde{\rho}'}{\partial \tilde{t}} + \tilde{\mathbf{v}} \cdot \tilde{\nabla}\tilde{\rho}'\right) + \left(\frac{L_d}{L}\right)^2 \tilde{w}\tilde{N}^2 = 0, \tag{10}$$

$$\tilde{\nabla}_h \cdot \tilde{\mathbf{v}}_h + \frac{\partial \tilde{w}}{\partial \tilde{r}} = 0. \tag{11}$$

Furthermore, we have introduced the baroclinic Rossby deformation radius L_d, given by

$$L_d = \frac{N_0 H}{\Omega}, \tag{12}$$

which is analogous to the deformation radius $\sqrt{gH}/\Omega$ in shallow water systems, such as that seen in Verkley [12] and Franken et al. [7].

One important aspect to highlight is that, although the equations are valid everywhere, this particular scaling is not strictly applicable in a narrow band around the equator. At very small latitudes, the Coriolis term decreases, and the pressure scaling can no longer be determined from Eq. (8) as $\tilde{f}$ becomes of the same order as the Rossby number. Specifically, the ratio between inertial forces and the Coriolis force is locally given by the local Rossby number $\mathrm{Ro}_{loc} = U/L\Omega \sin\phi = \mathrm{Ro}/\sin\phi$. In the regime of rapid rotation that we consider, the global Rossby number is very small, leading to a similarly small local Rossby number at moderate and high latitudes. The domain where the scaling is not applicable is thus contained in a very narrow equatorial band where the local Rossby number requirement for geostrophic flow $\mathrm{Ro}_{loc} \ll 1$ is not satisfied. In the following, we will continue with the non-dimensionalised equations, but the tildes will be omitted for clarity.

2.3. Geostrophic balance

In the regime of rapid rotation where the Rossby number is small, it can be seen directly from the momentum Eq. (8) that inertial forces are small, and that there is an approximate balance between the Coriolis force and the hydrostatic pressure force. In this case of strong scale separation, the flow is said to be in geostrophic balance [16]. In this section, we discuss the impact of the scale separation on the dynamics of the Boussinesq PE.

The non-dimensionalized Boussinesq PE reveal that the dynamics are dependent on the horizontal length scale L that is considered. The quasi-geostrophic approximation can be applied when the considered horizontal length scale of the flow is of the same order as the Rossby deformation radius, or, $L_d/L = \mathcal{O}(1)$. Typical values of L_d in geophysical flows depend on the application area. For example, in Earth's atmosphere this scale is typically of $\mathcal{O}(10^3)$ km, while in the Earth's upper ocean, this is of $\mathcal{O}(10-10^2)$ km [16]. Another possible application area is the atmosphere of Jupiter, for which $L_d \sim 2000$ km [19]. It should be noted that, especially in the latter two cases, we can consider length scales for which $L_d/L = \mathcal{O}(1)$ while having $L/R \ll 1$.

In a tangent plane approximation, the geostrophic balance is used to decompose the horizontal velocity field into its geostrophic and ageostrophic parts. The geostrophic velocity is found using the scale separation Eq. (8) by neglecting the inertial term:

$$f\hat{\mathbf{r}} \times \mathbf{v}_h + \nabla_h p' = 0. \tag{13}$$

However, this geostrophic velocity is ill-defined on the equator [9]. In [20,21] it is shown that one can instead look at the cross-derivative (or horizontal curl, or perpendicular divergence) to avoid pointwise evaluations of the geostrophic velocity at the equator. Taking the cross-derivative of the balance equation above, defined as a left-multiplication by $\hat{\mathbf{r}} \cdot \nabla\times$ gives

$$f\nabla_h \cdot \mathbf{v}_h + \mathbf{v}_h \cdot \nabla_h f = 0. \tag{14}$$

where we use the fact that the curl of a gradient field is zero everywhere. The first term contains the divergence of the horizontal part of the velocity field, while the second term contains the gradient of the nondimensional Coriolis parameter. Due to the non-dimensionalization, this is $\mathcal{O}(L/R)$. Thus, for the horizontal length scales around the baroclinic Rossby radius, this is a small quantity. The balance above thus implies that the horizontal velocity field is divergence-free to a good approximation. Instead of the typical decomposition of the velocity field into a geostrophic and an ageostrophic component, here we split the field into a dominant divergence-free field and a remaining term of small magnitude. Using the Helmholtz decomposition, we can therefore introduce a streamfunction ψ for the former part and write the velocity decomposition as

$$\mathbf{v}_h = \hat{\mathbf{r}} \times \nabla\psi + \epsilon \mathbf{v}'_h, \tag{15}$$

where $\epsilon \ll 1$ is a scaling parameter for the divergent part of the horizontal velocity field $\mathbf{v}'_h$. Since the total velocity field is still assumed to be divergence-free, we find from (11) that

$$\frac{\partial w}{\partial r} + \epsilon \nabla_h \cdot \mathbf{v}'_h = 0. \tag{16}$$

This implies that the vertical velocity is smaller than the suggested scaling of UH/L due to the presence of the small parameter ϵ. From this point, we can follow the same steps as in typical derivations on a local tangent plane. By cross-differentiating the horizontal momentum equation, i.e., applying $\hat{\mathbf{r}} \cdot \nabla\times$ to Eq. (8), we find

$$\mathrm{Ro}\left[\frac{\partial \zeta}{\partial t} + \mathbf{v}_h \cdot \nabla_h \zeta + \zeta \nabla_h \cdot \mathbf{v}_h + w\frac{\partial \zeta}{\partial r} - \hat{\mathbf{r}} \cdot \nabla_h w \times \frac{\partial \mathbf{v}_h}{\partial r}\right] + \mathbf{v}_h \cdot \nabla_h f + f\nabla_h \cdot \mathbf{v}_h = 0, \tag{17}$$

where we introduced the (scalar-valued) vorticity of the horizontal velocity field $\zeta := \hat{\mathbf{r}} \cdot \nabla \times \mathbf{v}_h$. Given the scaling assumptions above, we can neglect the fourth and fifth terms in the square brackets, since the vertical velocity is of $\mathcal{O}(\epsilon)$. Similarly, the third term is neglected due to the small divergence of the horizontal velocity. In the remaining terms, we now substitute the velocity decomposition (15) and neglect the non-divergent part in the advective terms. Defining a horizontal material derivative $\mathrm{D}/\mathrm{D}t(\cdot) = \partial(\cdot)/\partial t + \hat{\mathbf{r}} \times \nabla\psi \cdot \nabla_h(\cdot)$ now gives

$$\frac{\mathrm{D}}{\mathrm{D}t}(\mathrm{Ro}\,\zeta + f) + \epsilon(\mathrm{Ro}\,\zeta + f)\nabla_h \cdot \mathbf{v}'_h = 0, \tag{18}$$

using the fact that the Coriolis parameter is time-independent. Since the Rossby number is small, we can neglect the first term in the second brackets, and we introduce the divergence-free requirement (16) to find

$$\frac{\mathrm{D}}{\mathrm{D}t}(\mathrm{Ro}\,\nabla^2\psi + f) - f\frac{\partial w}{\partial r} = 0, \tag{19}$$

where we use the small value of ϵ in Eq. (15) to approximate the horizontal vorticity by the Laplacian of the streamfunction ψ. We can use the continuity Eq. (10) to eliminate the vertical velocity. By again neglecting the nondivergent part of the advecting horizontal velocity, we can rewrite the continuity equation as

$$\mathrm{Ro}\frac{\mathrm{D}}{\mathrm{D}t}\rho' + \left(\frac{L_d}{L}\right)^2 wN^2 = 0. \tag{20}$$

The above equation can be used to determine the vertical velocity w to be used in the vorticity evolution (19). By noting that the radial derivative commutes with the horizontal material derivative commutes, we can extract the vertical velocity by taking the radial derivative to find

$$\begin{aligned} f\frac{\partial w}{\partial r} &= -\mathrm{Ro}\left(\frac{L}{L_d}\right)^2 f\frac{\mathrm{D}}{\mathrm{D}t}\left(\frac{\partial}{\partial r}\left(\frac{\rho'}{N^2}\right)\right) \\ &= -\mathrm{Ro}\left(\frac{L}{L_d}\right)^2\left[\frac{\mathrm{D}}{\mathrm{D}t}\left(f\frac{\partial}{\partial r}\left(\frac{\rho'}{N^2}\right)\right) - \frac{\partial}{\partial r}\left(\frac{\rho'}{N^2}\right)\frac{\mathrm{D}f}{\mathrm{D}t}\right]. \end{aligned} \tag{21}$$

The second term between square brackets can be neglected since the Coriolis term f varies only slowly over the sphere which implies $\mathrm{D}f/\mathrm{D}t \sim \mathcal{O}(L/R)$. Combining Eqs. (13) and (15), we find that the pressure fluctuations are predominantly determined by the divergence-free part of the horizontal velocity field, such that we can approximate $p' = f\psi$ (up to a gauge constant). This result, combined with the hydrostatic pressure relation (9) allows us to write the density fluctuations in terms of the streamfunction, resulting in

$$f\frac{\partial w}{\partial r} = -\mathrm{Ro}\left(\frac{L}{L_d}\right)^2\frac{\mathrm{D}}{\mathrm{D}t}\left(f^2\frac{\partial}{\partial r}\left(\frac{1}{N^2}\frac{\partial\psi}{\partial r}\right)\right), \tag{22}$$

where we use the fact that the Coriolis parameter is independent of the radial coordinate in the shallow water assumption. Substitution of this result in the main dynamical Eq. (19) now gives stratified QG equations on the sphere

$$\frac{\mathrm{D}q}{\mathrm{D}t} = 0, \quad q = \mathrm{Ro}\,\nabla^2\psi + f + \mathrm{Ro}\left(\frac{L}{L_d}\right)^2 f^2\frac{\partial}{\partial r}\left(\frac{1}{N^2}\frac{\partial\psi}{\partial r}\right), \tag{23}$$

where q is the potential vorticity for the stratified QG equations, which is materially conserved on horizontal planes and is the single prognostic variable. Note the f^2 factor in the third term of the QG potential vorticity, which follows from the derivation of QG using the Helmholtz decomposition instead of the geostrophic/ageostrophic splitting. Since the stratified QG equations are an approximation of the PE, the potential vorticity q is an approximation of Ertel's potential vorticity for three-dimensional stably stratified flows. The model is completed with boundary conditions on the top and bottom layer. For atmospheric problems, usually one takes the bottom layer to be topography with a free boundary on the top, whereas for oceanic problems, usually one takes the top layer to be rigid and the bottom layer to be free. In the present work, we take rigid boundary conditions on both the bottom and the top. This final result is very similar to the traditional stratified QG equation on a Cartesian plane. Compared to the derivation in Cartesian coordinates in Ripa [22], the present equations differ in the crucial appearance of the fully latitude-dependent Coriolis term f. Buoyancy fluxes through the boundaries have not been included, though this can be achieved through modifying the boundary conditions appropriately. The main difference lies in the decomposition of the horizontal velocity in terms of a divergence-free contribution and a small divergent field. The geostrophic velocity can now be reconstructed from the streamfunction, which is well-defined on the entire sphere.

While the final formulation of the stratified QG equations on the sphere appears to be a straightforward generalization of the well-known formulation on the β-plane, its derivation sheds light on the applicability of the model on the sphere. Starting from the Boussinesq PE on the sphere, the geostrophic balance is used to derive the leading order dynamics in terms of the Rossby number. This is valid at all latitudes where a scale separation exists between the Coriolis force and inertial forces. It thus provides a continuous model for both mid-latitude and polar dynamics. At a narrow band around the equator, scale separation breaks down as the Coriolis parameter vanishes. In the absence of a local geostrophic balance, gravity waves play an important role and the QG equation does not provide accurate results for the dynamics [9]. From previous studies, e.g. Franken et al. [7] in comparison with Cifani et al. [8], we know that the Coriolis effect itself is enough to introduce alternating jets in rotating Euler and Navier-Stokes equations. The effect of the single-layer quasi-geostrophic approximation is to introduce a latitude-dependent modulation of the mean zonal velocity. One of the striking features that the single-layer QG model on the sphere identifies is the transition from a region of alternating jets near the equator towards regions of more isotropic turbulence. In the next section, we derive the multi-layer QG equations to incorporate the effects of vertical stratification.

2.4. Multi-layer stratification

From the continuous equations, a layered model may be derived by subdividing the domain vertically into horizontal layers. Within each layer, a constant density may be set, such that the density distribution over the layers approximates the continuous stratification that would appear in a full 3D formulation. This is equivalent to employing a finite-difference discretization in the radial direction [16], which will be the approach in this section. When the average density stratification is stable, its level sets (surfaces of constant density) form non-overlapping horizontal slices of the fluid column. In the derivations above, we assumed that density fluctuations are small compared to the average stratification, indicating that the isopycnals form approximately spherical shells. Thus we describe the fluid using several layers of constant thickness and uniform density given by the average stratification, whose interfaces correspond to isopycnals of the continuous model.

Using this approach, we divide the domain in the radial direction into M spherical shells. We denote the layers from top to bottom with index $j = 1, \dots, M$, where each layer has thickness H_j such that $\sum_{j=1}^{M} H_j = H$. We can describe the dynamics in each layer by the potential vorticity q_j and streamfunction ψ_j.

We can employ a second-order centered finite difference scheme to the radial derivatives in (23), similar to the approach taken in Vallis [16] for the β-plane equations. This yields the approximation

$$\frac{\partial}{\partial r}\left(\frac{1}{N^2}\frac{\partial \psi}{\partial r}\right) \approx \frac{1}{H_j}\left(\frac{1}{N^2_{j-\frac{1}{2}}}\frac{\psi_{j-1}-\psi_j}{H_{j+\frac{1}{2}}} - \frac{1}{N^2_{j+\frac{1}{2}}}\frac{\psi_j-\psi_{j+1}}{H_{j+\frac{1}{2}}}\right), \tag{24}$$

where $H_{j+\frac{1}{2}} = (H_{j+1}+H_j)/2$ and the Brunt-Väisälä frequencies are given by central differencing of Eq. (6) as

$$N^2_{j+\frac{1}{2}} = -\frac{g}{H_{j+\frac{1}{2}}}\frac{\rho_j-\rho_{j+1}}{\rho_0} = -\frac{g'_{j+\frac{1}{2}}}{H_{j+\frac{1}{2}}}, \quad \text{where} \quad g'_{j+\frac{1}{2}} = g\frac{\rho_{j+1}-\rho_j}{\rho_0} \tag{25}$$

where the reduced gravity $g'_{j+\frac{1}{2}}$ has been introduced as a measure of the effective gravitational acceleration between layers. Applying this discretization in the radial direction to the stratified QG Eq. (23), we find the multi-layer QG equations on the sphere

$$\dot{q}_j + \{\psi_j, q_j\} = 0, \quad j = 1, \dots, M \tag{26}$$

where q_j is the layerwise potential vorticity, given by

$$\mathbf{q} = \nabla^2\boldsymbol{\psi} + \mathbf{f} + A\boldsymbol{\psi}, \tag{27}$$

where $\mathbf{q} = [q_1, q_2, \dots, q_M]^\top$ is a vector containing the layer-wise PV, and similarly $\boldsymbol{\psi} = [\psi_1, \psi_2, \dots, \psi_M]^\top$ and $\mathbf{f} = [1, 1, \dots, 1]^\top f$. The interaction between layers is given by the matrix $A \in \mathbb{R}^{M\times M}$, which is given in terms of the reduced gravity and layer thickness as

$$A = \mathrm{Ro}\left(\frac{L}{L_d}\right)^2 f^2 \begin{bmatrix} -\frac{1}{g'_{3/2}H_1} & \frac{1}{g'_{3/2}H_1} & 0 & \ddots & 0 \\ \frac{1}{g'_{3/2}H_2} & -\frac{1}{g'_{3/2}H_2} - \frac{1}{g'_{5/2}H_2} & \frac{1}{g'_{5/2}H_2} & \ddots & 0 \\ 0 & \frac{1}{g'_{5/2}H_3} & -\frac{1}{g'_{5/2}H_4} - \frac{1}{g'_{7/2}H_4} & \ddots & 0 \\ \vdots & \ddots & \ddots & \ddots & \vdots \\ 0 & \cdots & \cdots & \cdots & -\frac{1}{g'_{M-1/2}H_L} \end{bmatrix}, \tag{28}$$

as follows directly from (23) using (24) and (25). Rigid lid boundary conditions are present in A. Different boundary conditions would lead to changes in the first and last row. The horizontal material derivative $\mathrm{D}/\mathrm{D}t$ has been rewritten using the canonical Poisson bracket on the sphere, which, in terms of the latitude ϕ and the longitude θ is given by

$$\{a, b\} = \frac{1}{R^2\cos\phi}\left(\frac{\partial a}{\partial\theta}\frac{\partial b}{\partial\phi} - \frac{\partial a}{\partial\phi}\frac{\partial b}{\partial\theta}\right) = (\hat{\mathbf{r}} \times \nabla a)\cdot\nabla b. \tag{29}$$

From this formulation of horizontal PV transport in terms of the canonical Poisson bracket on the sphere, we note the layerwise similarity to the single-layer QG equation as described on the sphere Verkley [12] and Schubert et al. [11]. In particular, the only difference appears in the relation between streamfunction and potential vorticity (27).

Recently, the Poisson structure of the single-layer QG equation on the sphere has been discussed in Franken et al. [7]. From their analysis, we find that (26) constitutes a Lie–Poisson system on the space of smooth functionals on the sphere $C^\infty(S^2)$ for each layer separately, where the Lie–Poisson bracket is given in terms of the canonical Poisson bracket by

$$\{\mathcal{A}, \mathcal{B}\}_{LP}(q) = \int_{S^2} q\left\{\frac{\delta\mathcal{A}}{\delta q}(q), \frac{\delta\mathcal{B}}{\delta q}(q)\right\}\mathrm{d}x, \tag{30}$$

with $\mathcal{A}, \mathcal{B} : C^\infty(\mathbb{S}^2) \to \mathbb{R}$ smooth functionals and $\mathrm{d}x$ is an infinitesimal area element, which, in latitude-longitude coordinates is given by $\mathrm{d}x = R\cos\phi\,\mathrm{d}\phi\,\mathrm{d}\theta$. The advection of layer-wise PV (26) may thus be more generally written as

$$\frac{\mathrm{d}}{\mathrm{d}t}\mathcal{F}(q_j) = \{\mathcal{F}(q_j), \mathcal{H}(q_j)\}_{LP}, \tag{31}$$

with the Hamiltonian functional given by

$$\mathcal{H}(q) = -\frac{1}{2}\sum_{j=1}^{M}\int_{S^2}\psi_j(q_j - f)\,\mathrm{d}x. \tag{32}$$

Thus, similar to the single-layer QG equations, this system allows for infinitely many conserved quantities in the form of Casimir functionals $\mathcal{C} : C^\infty(S^2) \to \mathbb{R}$ for which holds

$$\{\mathcal{F}(q_j), \mathcal{C}(q_j)\}_{LP} = 0, \quad \forall\mathcal{F} : C^\infty(S^2) \to \mathbb{R}, \tag{33}$$

which in this case results in $\mathcal{C}(q_j) = \int_{S^2}\zeta(q_j)$ for any smooth function $\zeta \in C^\infty(\mathbb{R})$, which indicates that for each layer, any integrated function of potential vorticity is a constant of motion. This may be verified by direct computation

$$\begin{aligned} \frac{\mathrm{d}}{\mathrm{d}t}\mathcal{C}(q_j) &= \int_{S^2}\dot{q}_j\zeta'(q_j)\mathrm{d}x = -\int_{S^2}\left((\mathbf{u}_j)_h\cdot\nabla q_j\right)\zeta'(q_j)\mathrm{d}x \\ &= -\int_{S^2}(\mathbf{u}_j)_h\cdot\nabla\zeta(q_j)\mathrm{d}x = \int_{S^2}\nabla\cdot(\mathbf{u}_j)_h\zeta(q_j)\mathrm{d}x \\ &= 0. \end{aligned} \tag{34}$$

Typically, only integrated monomials of PV are considered since they form a basis for functions on the sphere. In particular, the integrated square of PV is called the total enstrophy, and plays an important role in the characterization of geophysical fluid dynamics [23,24]. As previously noted in Franken et al. [7], this conservative property is independent of the specific relation between streamfunction and potential vorticity. This explains the similarity in the constants of motion between this model and other incompressible 2D flows such as the 2D Euler equations and the rotating shallow water equations. For a detailed overview of the relation between these models, we refer to Luesink [25].

In the next section, we use the approach of Zeitlin [26] to apply a spatial discretization that preserves as many Casimirs of the continuous system as possible. By choosing a suitable time integrator, these Casimirs may then be conserved in a numerical solution, allowing us to study the importance of higher-order moments of PV.

3. Numerical method

In the previous section, the multi-layered QG equations on the sphere were derived, resulting in a dynamical equation for potential vorticity q, in terms of the streamfunction ψ . This system features an infinite family of constants of motion due to the Lie–Poisson property of the dynamical system.

In this section, we present an extension of the single-layer QG discretization [7]. The resulting multi-layer description is augmented with a preconditioner for multi-layer QG [27] and a geometric method for two-dimensional hydrodynamics [28]. This combination of techniques yields an efficient computational method for the multi-layered QG equations that is the main novelty of the current study. Namely, we construct a numerical method for solving this system that preserves the Lie–Poisson structure in order to retain as many constants of motion as possible in the numerical solution. The method of lines is used, where we first project functions on the sphere onto a particular discrete basis such that the resulting system of ODEs is Lie–Poisson. Then, a suitable time integrator is selected to conserve the Casimirs of the discrete system as well as the associated Hamiltonian energy. These aspects are presented in detail below.

3.1. Spatial discretization

The construction of a projection of the infinite-dimensional Lie–Poisson system (31) to a finite-dimensional Lie–Poisson system was first employed in Zeitlin [26]. This was motivated by a projection method on a flat geometry in Zeitlin [29] for the 2D Euler equations. Since the potential vorticity evolves by the Lie–Poisson bracket, it is an element of the associated Poisson algebra. The projection method is based on a finite-dimensional approximation of the Lie–Poisson bracket. Since a finite-dimensional Lie algebra can always be written as a matrix algebra, the method consists of constructing a matrix Lie algebra of dimension $(N \times N)$, such that the sequence approximates the infinite-dimensional Poisson algebra as N goes to infinity. This convergence is defined in terms of the structure constants of a basis of the algebra. In other words, a sequence of Lie algebras is said to converge to the infinite-dimensional Poisson algebra $C^\infty(S^2)$ if the structure constants of the matrix bases converge to that of the spherical harmonics basis $Y_{l,m}$ of $C^\infty(S^2)$. As was shown for a general case in Bordemann et al. [30], and later for the spherical geometry by Zeitlin [26] based on the work of Hoppe [31], such a sequence exists, given by the basis $T_{l,m}$ for the matrix Lie algebra $\mathfrak{u}(N)$, i.e., the algebra of skew-Hermitian matrices. Given a function $a \in C^\infty(S^2)$ written in terms of the basis as $a = \sum_{l=0}^{\infty} \sum_{m=-l}^{l} a_{l,m} Y_{l,m}$, the implied projection $\Pi_N : C^\infty(S^2) \to \mathfrak{u}(N)$ is then given by

$$\Pi_N a = A := \sum_{l=0}^{N-1} \sum_{m=-l}^{l} i a_{l,m} \hat{T}_{l,m}, \tag{35}$$

where the modified basis $\hat{T}_{l,m}$ follows directly from the complex part of $T_{l,m}$ as detailed in Cifani et al. [6]. Similar to their infinite-dimensional counterparts, $\hat{T}_{l,m}$ are eigenfunctions of the Laplace operator, which, in this case, is the discrete Laplace operator on the sphere Δ_N as provided by Hoppe and Yau [32]. Thus, the basis matrices are calculated by solving the eigenvalue problem

$$\Delta_N \hat{T}_{l,m} = l(l+1)\hat{T}_{l,m} \tag{36}$$

Although the discrete Laplacian is a fourth-order tensor, it operates independently on diagonals of a matrix. Thus, the tensor splits into $(2N-1)$ blocks $\Delta_N^{(m)}$ of size $N - |m|$. Moreover, these blocks are tridiagonal given as

$$\begin{aligned}(\Delta_N^{(m)})_{ij} &= 2\delta_i^j (s(2i+1+m) - i(i+m)) \\ &\quad -(\delta_{i+1}^j + \delta_i^{j+1})\sqrt{(i+1+m)(i+1)}\sqrt{(N-1-i-m)(N-1-i)},\end{aligned} \tag{37}$$

where $s = (N-1)/2$ and $i, j = 0, \dots, N-m-1$. This sparse structure of the discrete Laplace operator can be inverted using $\mathcal{O}(N^2)$ operations, which has enabled efficient numerical solvers such as that reported in Cifani et al. [6] on which the current numerical framework is built. As the discrete Laplacian splits into independent blocks acting along diagonals of a matrix, it follows that the matrices T_{lm} can be represented as $(N - |m|)$-dimensional complex vectors, occupying the m-th diagonal of an otherwise empty matrix.

The similarity between the structure constants of the discrete basis T_{lm} and those of Y_{lm} in the continuous case also results in a close relation between the Poisson bracket (29) and the Lie bracket on $\mathfrak{u}(N)$, which is the matrix commutator. The

$$\Pi_N\{f, g\} = [\Pi_N f, \Pi_N g]_N + \mathcal{O}(N^{-2}), \tag{38}$$

where $[A, B]_N = N^{3/2}/\sqrt{16\pi}\,(AB - BA)$ is the rescaled matrix commutator [30,33]. Using the explicit projection in (35), we introduce the layerwise potential vorticity matrices Q_j and associated stream matrices P_j using

$$Q_j = \sum_{l=0}^{N-1} \sum_{m=-l}^{l} i(q_j)_{lm} \hat{T}_{lm}^{(N)}, \quad \text{and} \quad P_j = \sum_{l=0}^{N-1} \sum_{m=-l}^{l} i(\psi_j)_{lm} \hat{T}_{lm}^{(N)}, \quad j = 1, \dots, M \tag{39}$$

Similarly, we introduce the Coriolis matrix $F := \Pi_N f$ and its square $S := \Pi_N f^2$, which allows us to derive the spatial discretization of (26) and (27) as

$$\dot{Q}_j = -[P_j, Q_j] \quad j = 1, \dots, M \tag{40}$$

with potential vorticity given in terms of the stream matrices as

$$Q_j = \Delta_N P_j + F + \tilde{S} \circ \left(\sum_{k=1}^{M} A_{jk} P_k \right) \quad j = 1, \dots, M \tag{41}$$

where the projection of the product $f^2\psi$ is given by the operation $\tilde{S}\circ P$ with $\circ$ denoting element-wise multiplication, as was derived in Franken et al. [7]. The matrix $\tilde{S}$ is given by

$$\tilde{S}_{kl} = -\frac{i}{2}\sqrt{\frac{N}{4\pi}}(S_{kk} + S_{ll}), \tag{42}$$

where S_{kk} and S_{ll} denote the kth and lth diagonal entries of S, respectively. System (40) constitutes M isospectral equations. They are Lie–Poisson with respect to the Lie algebra $\mathfrak{u}(N)$ with the Lie bracket $[\cdot,\cdot]$, for which the Casimirs $C_{j,k}$ by isospectrality are given as

$$C_{j,k} = \mathrm{trace}\big((Q_j)^k\big), \quad k = 0, 1, \dots, N-1, \quad j = 1, \dots, M, \tag{43}$$

which indicates that integrated monomial functions of potential vorticity is conserved in each layer, similar to the dynamics of a single-layer QG model.

Solving the system of Eq. (40) now requires a suitable time integration method, as well as a method for calculating the stream matrices P_j from the implicit relation given in (41), which is discussed in the following two subsections.

3.2. Calculation of the streamfunctions

Since the main dynamical variable in the evolution of multi-layer quasi-geostrophic flow is the potential vorticity, the resulting velocity field, which in turn is calculated from the stream function, must be determined using the implicit relation (41). In the special case where the interaction matrix A is zero, i.e., in the absence of density stratification, the horizontal velocity field in each layer is independent and the stream matrix can be determined using

$$P_j = (\Delta_N)^{-1}(Q_j - F), \quad j = 1, \dots, M. \tag{44}$$

Recall that M denotes the number of layers in the multilayer model. Similar to the observation that the streamfunction is uniquely determined only up to a constant function on the sphere, the discrete Laplacian is only invertible when adding an additional constraint on the stream matrix. For convenience, we may set $\int_{S^2}\psi_j = 0, \forall j = 1, \dots, M$, which corresponds in the discrete case to the constraint

$$\mathrm{trace}(P_j) = 0, \quad j = 1, \dots, M \tag{45}$$

Using the diagonal splitting of the discrete Laplacian, the calculation (44) can be performed using $\mathcal{O}(N^2)$ operations following [6].

Under the influence of density stratification, the stream matrices no longer decouple between layers, and the fully coupled system (41) needs to be considered. For a general interaction matrix, this involves solving a system of M coupled elliptic equations of size $N \times N$. However, in many cases, the matrix A is diagonalizable, leading to an ideal pre-conditioner for the coupled system.

If the matrix A is diagonalizable, then there exist an invertible square matrix V and a diagonal matrix D such that

$$A = VDV^{-1}. \tag{46}$$

Substitution of this decomposition into Eq. (41) then gives

$$\hat{Q}_k = \Delta_N \hat{P}_k + F + \tilde{S}\circ\big(D_{kk}\hat{P}_k\big), \quad k = 1, \dots, M, \tag{47}$$

where $\hat{Q}_k = \sum_{j=1}^{M} V_{kj}^{-1} Q_j$ and $\hat{P}_k = \sum_{j=1}^{M} V_{kj}^{-1} P_j$ are the potential vorticity matrices and stream matrices respectively corresponding to the modes of the system [27]. Crucially, the potential vorticity matrix $\hat{Q}_j$ associated with a particular mode j is independent of the other modes. Thus, system (47) constitute M independent implicit equations for the stream matrices $\hat{P}_j$, which can be made explicit by solving

$$\hat{P}_k = \big(\Delta_N + D_{kk}\tilde{S}\circ\big)^{-1}(\hat{Q}_k - F), \quad k = 1, \dots, M, \tag{48}$$

which can be solved efficiently in just $\mathcal{O}(N^2)$ operations using the scheme based on diagonal splitting as developed in Franken et al. [7]. The layerwise PV and streamfunction matrices can then be reconstructed using the relations

$$Q_j = \sum_{k=1}^{M} V_{jk}\hat{Q}_k, \quad P_k = \sum_{k=1}^{M} V_{jk}\hat{P}_k \tag{49}$$

In the case where the interaction matrix A is not diagonalizable, there is no such decomposition into independent modes. However, the stream matrices can still be calculated directly from Eq. (41) using diagonal splitting. If we denote the m-th diagonal of a matrix by the superscript $\cdot^{(m)}$ as a row vector, we may introduce the column vectors $P^{(m)}, Q^{(m)} \in \mathbb{C}^{(N-|m|)L}$ as

$$\mathbb{P}^{(m)} = \begin{bmatrix} P_1^{(m)} & P_2^{(m)} & \cdots & P_L^{(m)} \end{bmatrix}^\top \tag{50}$$

and

$$Q^{(m)} = \begin{bmatrix} Q_1^{(m)} & Q_2^{(m)} & \cdots & Q_L^{(m)} \end{bmatrix}^\top, \tag{51}$$

which allows us to decompose the entire system (41) into its diagonals as

$$(\mathbb{L}^{(m)} + \mathbb{S}^{(m)})P^{(m)} = Q^{(m)} - F^{(m)}, \quad m = -(N-1), \dots, N-1 \tag{52}$$

using the matrix operators $\mathbb{L}^m, \mathbb{S}^m \in \mathbb{C}^{[(N-|m|)M]\times[(N-|m|)M]}$ given as

$$\mathbb{L}^{(m)} = I_M \odot \Delta_N^{(m)} \tag{53}$$

and

$$\mathbb{S}^{(m)} = A \odot \tilde{S}^{(m)} \tag{54}$$

where $\odot$ denotes the Kronecker product and I_M is the identity matrix of dimension M. The matrix $(\mathbb{L}^{(m)} + \mathbb{S}^{(m)})$ is extremely sparse with only 5 nonzero diagonals as can be seen from Eqs. (28) and (37). These can be solved efficiently using appropriate pre-conditioners [34] or using iterative methods. Here we note that in the case of a diagonalizable matrix A, the preconditioner can be found from the decomposition (46), which leads directly to system (48). Note that one only needs to solve for the diagonals $m \geq 0$, since the matrices P_j are skew-Hermitian. The linear scaling of the computational complexity with the number of layers facilitates simulations at high horizontal resolutions, similar to previous work on barotropic QG flow as reported by Franken et al. [7].

3.3. Time integration method

The evolution of the dynamical system is carried out by solving Eq. (40) in time. Analogous to the conservation of integrated functions of potential vorticity in the continuous system, this system of ODEs preserves the trace of polynomial functions of Q_j up to polynomial order $(N-1)$ as indicated in Eq. (43) for each layer. This property is equivalent to the spectrum of the layer-wise potential vorticity matrix being conserved [35], indicating that the evolution in (40) is isospectral.

This property is similar to the isospectral evolution of the potential vorticity matrix in a single-layer QG model as in Franken et al. [7], where it was also remarked that the isospectral property holds independent of the choice of advecting stream matrix. Therefore, we can select the same time-integration method to conserve the matrix spectrum on a discrete level.

We employ the time integrator as formulated in Modin and Viviani [36], based on second-order symplectic midpoint integration. This integrator falls within the class IsoSyRK methods, which are both symplectic and isospectral [37]. Given the solution Q_j^n at time t_n, the solution of (40) at time $t_{n+1} = t_n + h$ can then be written as follows

$$\begin{cases} \tilde{Q}_j = Q_j^n + \frac{h}{2}\left[\tilde{P}_j, \tilde{Q}_j^n\right] + \frac{h^2}{4}\tilde{P}_j\tilde{Q}_j\tilde{P}_j \\ Q_j^{n+1} = \tilde{Q}_j + \frac{h}{2}\left[\tilde{P}_j, \tilde{Q}_j\right] - \frac{h^2}{4}\tilde{P}_j\tilde{Q}_j\tilde{P}_j, \end{cases} \tag{55}$$

where $\tilde{P}_j$ is the stream matrix corresponding to the potential vorticity matrix $\tilde{Q}_j$ as given by Eq. (41). The integration thus consists of two steps. The first equation gives an implicit relation for the intermediate step $\tilde{Q}_j$, which is solved using fixed point iteration. This creates a sequence $\left\{\tilde{Q}_j^k\right\}$ with $\tilde{Q}_j^0 = Q_j^n$. All values of j have to be considered simultaneously at each iteration: $\tilde{Q}_j$ is needed to compute $\tilde{P}_j$, which in turn is needed to compute the stream matrix in other layers due to the coupling between the layers as seen in Eq. (49) The time step h is chosen sufficiently small such that the sequence converges to $\tilde{Q}_j$ as $k \to \infty$, and the iterative process terminates when all sequences have converged to within a set tolerance. For the chosen time step sizes h, the L_∞ norm of $\tilde{Q}_j^{k+1} - \tilde{Q}_j^k$ typically reaches $\mathcal{O}(10^{-8})$ after only 4 or 5 iterations.

Combining the described discretization methods and preconditioner for the streamfunction calculation leads to a numerical method which can be used for simulations even on personal computers. All presented results are obtained from simulations carried out in Matlab on the CPU of a personal laptop. We provide a rough estimate of the simulation runtimes in this setting. A three-layer simulation at resolution $N = 1024$ took approximately 13 h for 1.2×10^4 time steps, or roughly 3 seconds per time step. A four-layer simulation at $N = 256$ with 10^4 time steps was carried out in approximately one hour, taking around three time steps per second. Naturally, a speed-up is possible using, e.g., parallel computing (see [6]) which is the subject of current research efforts.

4. Simulation of multi-layer geostrophic turbulence

In this section, we demonstrate the capabilities of the developed numerical method by simulating two types of geophysical flows enabled by this method. In Section 4.1, we study the emergence of zonally elongated structure in the flow from random initial data in an energy- and enstrophy-conserving setting for a six-layer model. Section 4.2 presents results of forced geostrophic turbulence for a three-layered setting, where we compare the resulting velocity fields and energy spectra to those of single-layer QG turbulence.

4.1. Unforced turbulence

To verify the structure-preserving properties of the numerical methods, we perform a simulation of geostrophic turbulence in the absence of forcing, dissipation and friction. We consider an aqua planet (an idealized planet without topographic features [38]) of radius $R = 1000$ km, rotating with a period of 10^4 s. For a typical rms velocity of 0.2 m/s achieved in this simulation, this leads to a global Rossby number of $\mathrm{Ro} = V_{rms}/R\Omega \approx 3 \times 10^{-4}$, which is well within the geostrophic regime [19]. The fluid layer is decomposed into 6 layers of equal thickness set to $H_j = 2$ km. A strong stratification is imposed between the layers by setting the reduced gravities at the layer interfaces to $0.8, 0.6, 0.4, 0.2$ and 0.1 from top to bottom, indicating that the density gradient is largest in the top layers. This choice of parameters leads to baroclinic Rossby radii of $91, 45, 32, 24$ and 15 km.

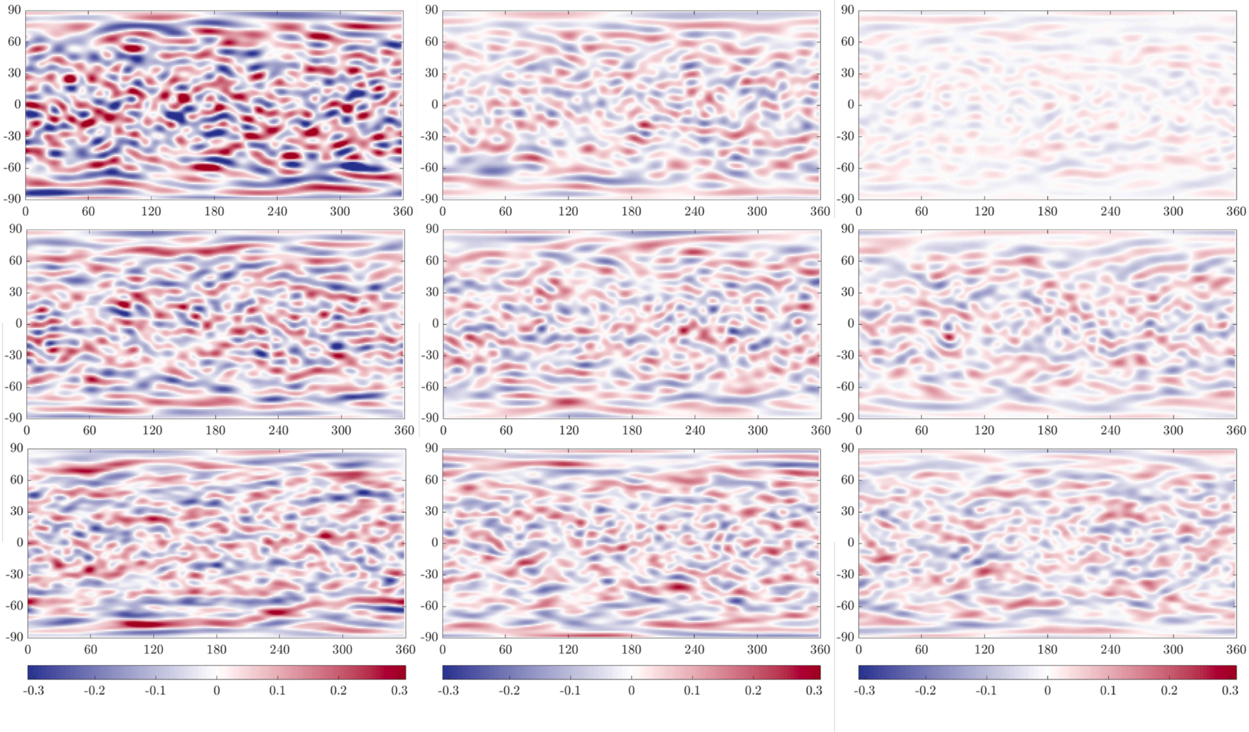

Fig. 1. Instantaneous zonal velocity fields for the energy and enstrophy-conserving setup. From left to right, the velocity fields of layers 1, 2 and 6 are visualized on a latitude-longitude grid. The velocity fields are calculated at $t = 0$ (top), $t = 2500$ 'days' (middle) and $t = 30,000$ 'days' (bottom).

A random initial large-scale velocity field is imposed in the top layer, and similarly at smaller amplitudes in lower layers. Similar to the work of [6], this is done by selecting the spherical harmonics modes with $1 < l < 30$ of all stream functions and giving them a random phase and a normally distributed amplitude around the value $\psi_0/l(l+1)$. The reference value $\psi_0 = 2 \times 10^{-4}/j$ is tuned such that the maximum jet velocity in the top layer is close to unity, with j the layer number ensuring that lower layers have a lower starting velocity scale. With this setup, the radial transfer of kinetic energy can be studied as the flow develops and kinetic energy is exchanged between the different layers. We simulate at a horizontal resolution of $N = 128$ during a period of 3×10^4 'days' (number of revolutions of the sphere), with an integration time step of $\Delta t = 10^3$ s, which implies a temporal resolution of 10 time steps per 'day'.

Fig. 1 shows several snapshots of the zonal component of the velocity field. The top row shows the initial zonal velocity of layers 1, 2 and 6, which are the top layer, second layer and bottom layer respectively. These initial velocity fields contain all spherical harmonics modes with degree $l \leq 30$, with a decreasing amplitude for lower layers. As the fluid evolves, two effects are visible in the zonal velocity snapshots. The second row in Fig. 1 shows the snapshots after 2500 'days', with the third row showing a snapshot after 30,000 'days'. The first effect is a migration of kinetic energy from the top layer to lower layers due to the interaction between layers. Layerwise, this represents a shift in the energy level at a constant Casimir surface. In other words, kinetic energy is transported between layers whilst enstrophy is conserved in each layer. The second effect is the evolution of potential vorticity within each layer. Small-scale structures are formed with $l > 30$ due to the nonlinear interactions between large-scale modes. The formation of zonal jet is not as pronounced as in the case of forced turbulence (Section 4.2). The baroclinic Rossby radii are large compared to the radius of the sphere such that baroclinic effects dominate the flow. However, the influence of baroclinic effects on jet formation is not well understood (see for example [39,40]) and demands further study, which is beyond the scope of this work.

The transfer of kinetic energy between layers is visualized in Fig. 2, showing the kinetic energy in each layer as a function of time in arbitrary units. The initial total energy per layer is determined via the amplitude of the random initial fields, leading to an initial kinetic energy proportional to j^{-2} where j is the layer number. The figure shows a transient phase up to approximately 2500 'days' of simulation during which kinetic energy is gradually transferred from the top layers towards the lower layers. After that, a stable distribution was reached which persists even after a very long time integration in which the top layers are only marginally more dynamically active than the lower layers due to the strong interaction between layers.

Finally, we illustrate the Casimir conserving property of the numerical method in Fig. 3, which shows the time evolution of several Casimirs for layers 1, 2 and 6 (from left to right). The figures show the relative error in the value of the first 16 Casimirs as a function of time, as given in Eq. 43. The relative error of the Casimirs is given in terms of their respective initial values and is displayed using increasingly light hues of grey for higher-order Casimirs. We find similar results as those reported in Franken et al. [7] for single layer QG dynamics in the Casimir-preserving setting. This includes the second-order Casimirs, representing the total enstrophy in each

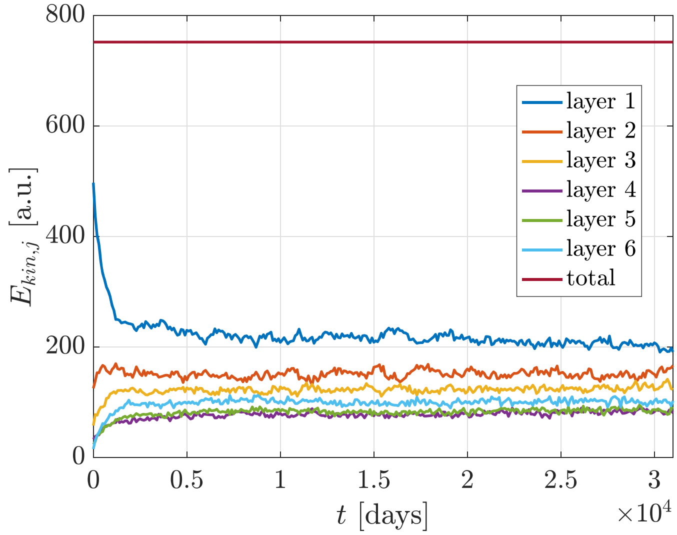

Fig. 2. Time evolution of the layer-wise kinetic energy in arbitrary units. The initial condition is chosen such that $E_{kin,j} \sim j^{-2}$, where j is the layer number. As the system evolves, kinetic energy is redistributed between the layers due to the interaction at the interfaces, and after approximately 2500 'days', the flow settles into a statistically stationary state with a stable kinetic energy distribution. The total energy is conserved up to relative fluctuations of order $\mathcal{O}(10^{-5})$.

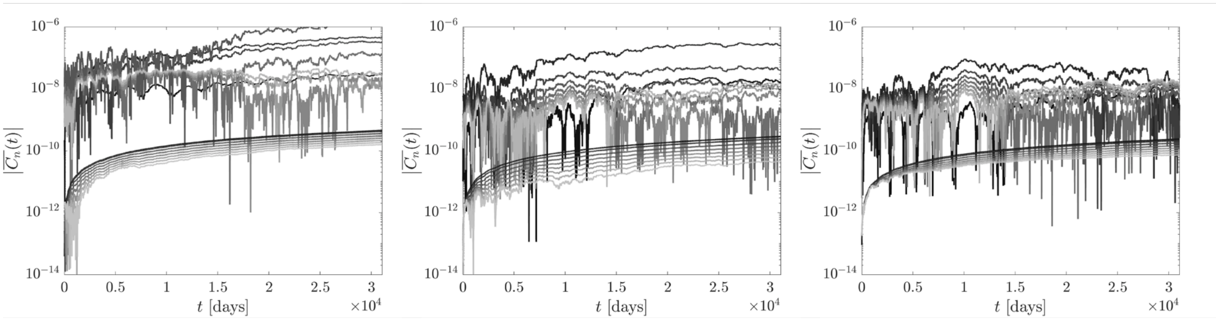

Fig. 3. Evolution of the relative error in the first 16 Casimirs in the system for the top layer (left), second layer (middle) and bottom layer (right). Successively higher order Casimirs are plotted using a lighter hue of gray, with even-order Casimir clustering around a relative error of 10^{-10} and odd-order Casimir displaying a relative error on the order of 10^{-8}.

layer. The odd-order Casimirs display an error of approximately 10^{-8}, (55). These results confirm that the numerical method indeed conserves all discrete Casimirs up to a very high precision.

The level of conservation is determined by the tolerance of the fixed point iteration, currently set to 10^{-10}, and the accuracy with which the basis elements T_{lm} are constructed. Further increasing (relaxing) the tolerance level leads to less well conserved Casimirs, whereas no significant changes were observed when decreasing the tolerance levels. This suggests that convergence of the iterative procedure is full and accuracy is limited by inherent aspects of the computations. A feature of particular relevance is the computation of the basis elements T_{lm}, of which numerical results suggest a large condition number. Finally, the precision with which the odd-order Casimirs are computed is less than that of the even-order Casimirs. This may well be related to the fact that odd-order Casimirs involve integration where, because of sign-changes in the integrand, a higher condition number arises and correspondingly precision is lost.

4.2. *Forced turbulence*

Many geophysical flows, such as the Earth's ocean and atmosphere, are heavily dependent on external forcing and are subject to dissipative effects in potential vorticity [41]. Examples of external forcing are wind shear on the upper ocean or thermal forcing from radiation [9]. Dissipation of potential vorticity occurs at small length scales beyond the geostrophic regime due to unresolved physical processes. This effect is typically modelled using an eddy viscosity term, see for example [4,42,43]. Furthermore, in the case of modelling oceanic flow, or the wind layer on other planets, the interaction between the bottom layer and the unresolved deep ocean is modelled with an Ekman boundary layer which corresponds to a linear drag force on the bottom layer [15,44]. These terms can be introduced into the PV evolution Eq. (26) as follows [4]

$$\dot{q}_j + \{\psi_j, q_j\} = \delta_{1,j} F_w - \delta_{j,N} \mu \Delta \psi_j + \nu \Delta^2 \psi_j, \tag{56}$$

where $\delta_{i,j}$ is the Kronecker symbol, F_w is the (wind) forcing acting only on the top layer, μ is the Ekman drag coefficient for the bottom friction layer and ν is the eddy viscosity. Similar to the approach taken in Thiry et al. [27], we integrate the terms on the righthand side of (56) using a third-order total variation diminishing Runge-Kutta (TVD-RK3) scheme. Given an ordinary differential equation

$$\dot{y}(t) = f(y(t)), \tag{57}$$

the scheme can be written as the following three-stage process

$$\begin{aligned} y^{(1)} &= y^{(0)} + h f(y^{(0)}) \\ y^{(2)} &= y^{(1)} + \frac{h}{4}\big(f(y^{(1)}) - 3f(y^{(0)})\big) \\ y^{(3)} &= y^{(1)} + \frac{h}{12}\big(8f(y^{(2)}) - f(y^{(1)}) - f(y^{(0)})\big), \end{aligned} \tag{58}$$

where h is the adopted time step size. The full system (56) can then be solved using an operator splitting method. By denoting the isospectral time integration map (55) for the advection term as $\varphi_{iso,h}$ for a time step of size h, and similarly denoting the TVD-RK3 integration map with $\varphi_{RK,h}$, we use a second-order Strang operator splitting to complete a full time stepping map φ_h using the composition

$$\mathbf{Q}^{k+1} = \big(\varphi_{RK,h/2} \circ \varphi_{iso,h} \circ \varphi_{RK,h/2}\big) \mathbf{Q}^k \tag{59}$$

where $\mathbf{Q}^k$ denotes the solution at time t_k, where $t_{k+1} = t_k + h$. Using this composition, the full dynamical Eq. (56) can be solved while retaining the structure-preserving integration for the nonlinear advection term, even though the full system does not conserve energy or Casimirs due to the forcing and dissipation processes.

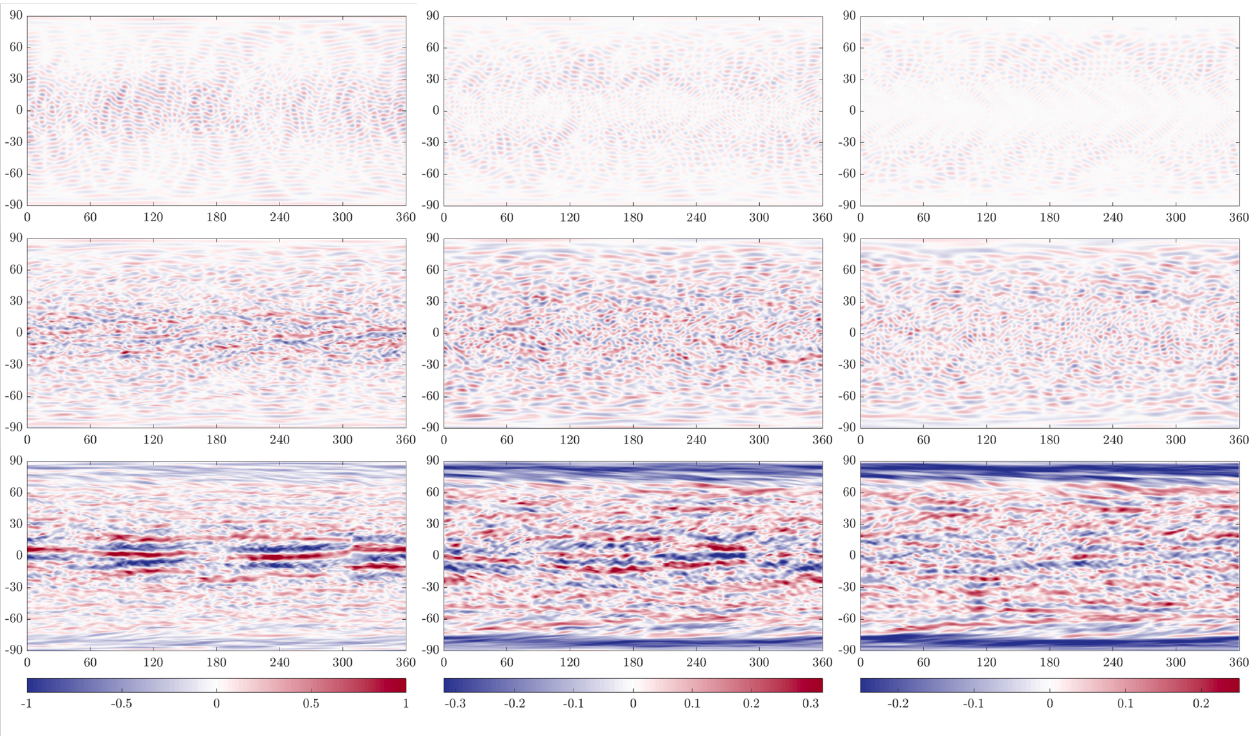

Fig. 4. Snapshots of the zonal component of the layer-wise velocity fields at several times. From top to bottom, snapshots are taken at $T = 140$ ‘days’, $T = 700$ ‘days’ and $T = 2100$ ‘days’. The flow develops from an initially stationary situation due to the random forcing on the top layer. In the figure, the left column shows the top layer zonal velocity field, the middle column shows the second layer and the right column shows the bottom layer. Note the different colour scales for the columns to visualize the resulting flow fields more clearly. The top row shows a snapshot after 140 ‘days’, which shows the development of small-scale flow structures at the length scale of the random forcing. The middle row shows the solution after 700 ‘days’, at which point the top layer clearly shows the emergence of elongated structures in the zonal direction. These develop further into the clear zonal jets shown after 2100 ‘days’ on the bottom row of the figure.

For this experiment, we localize the forcing F_w around a narrow band in spectral space around harmonics of degree $l = 50$ as is often used for studying homogeneous turbulence [8,45]. The remaining parameters of this simulation are based on the double-gyre experiment reported in Thiry et al. [27]. This experiment aims to simulate the emergence of a double wind-driven gyre on a tangent plane to study the westward jet between the gyres emanating from the eastern domain boundary. In our global fluid domain, the absence of north-south boundaries prevents us from replicating this experiment. Therefore, we use the aforementioned isotropic forcing to induce turbulent flow in the top layer, and the results for the multilayer system will be compared to the single-layer QG model presented in Franken et al. [7].

In this paper we focus on a novel computational model for a multi-layer QG formulation and adopt parameters relevant for the Earth's dynamics. We conveniently choose typical values as there is some uncertainty regarding the precise values for the Earth. In fact, we do not aim for an explicit comparison of our predictions with field observations. This is subject of ongoing study and will be published elsewhere. The fluid domain represents the Earth as an aqua-planet, for which we adopt $R = 6 \times 10^6$ m and a rotational period of the planet of $T = 86,400$ s. The experiment models oceanic flow with typical horizontal velocities of 0.5 m/s, leading to a global Rossby number of 10^{-3}. We consider a three-layer system with a layer thickness of $H_1 = 400$ m, $H_2 = 2000$ m and $H_3 = 4000$ m. The reduced gravities of the interfaces are set to 0.4 and 0.2 m/s^2, leading to baroclinic Rossby radii of 152 and 249 km respectively.

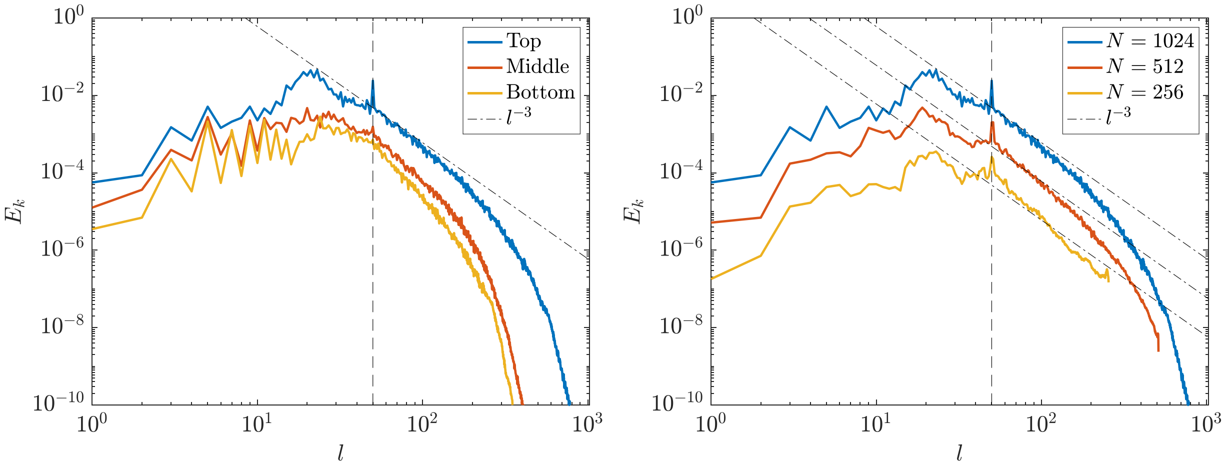

Fig. 5. Left: Kinetic energy profiles for all three layers at $T = 2100$ days at resolution $N = 1024$. For reference, the forcing wavenumber $l = 50$ is denoted with a dashed line, and the characteristic slope of l^{-3} is shown for reference. Right: Kinetic energy profile of the top layer at three different resolutions at $T = 2100$ days. For clarity, the energies at resolutions $N = 512$ and $N = 256$ are scaled by a factor 10 and 100, respectively.

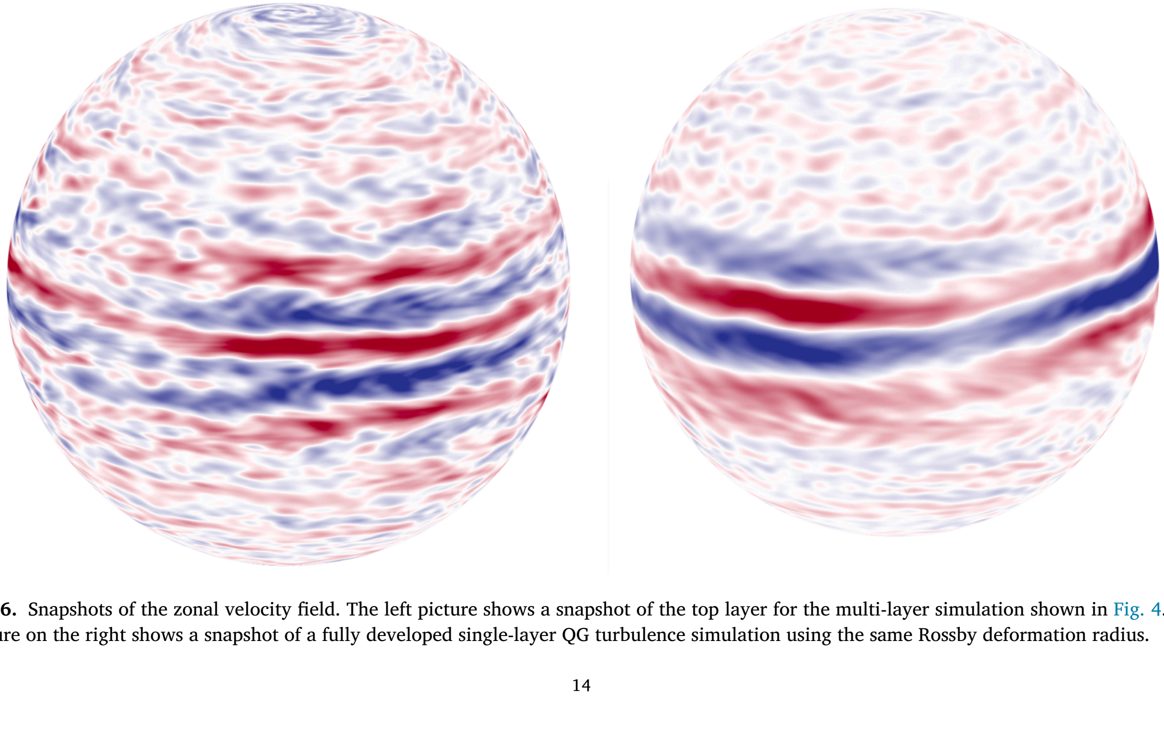

Fig. 6. Snapshots of the zonal velocity field. The left picture shows a snapshot of the top layer for the multi-layer simulation shown in Fig. 4. The picture on the right shows a snapshot of a fully developed single-layer QG turbulence simulation using the same Rossby deformation radius.

The eddy viscosity is set to $\nu = 60\,\mathrm{m}^2/\mathrm{s}$ following [8], and the Ekman drag coefficient is set to $\mu = 0.01\,\mathrm{s}^{-1}$ similar to Thiry et al. [27]. The spatial resolution is set to $N = 1024$ such that the smallest resolved length scale is approximately 10 km. This is significantly smaller than the baroclinic Rossby radii, thus ensuring that baroclinic waves are well-resolved [4]. The time step size is set to 10^3 s, resulting in approximately 87 time steps per day, with a total simulation time set to 2100 'days'. For comparison purposes, we also simulate a single layer QG system with the same parameters by setting the number of layers to 1. The influence of the geostrophic balance is maintained by retaining the value of $A(1,1)$ in Eq. (27). This is equivalent to a one-way interaction of the (single) top layer with a stationary deep ocean.

As is clear from the simulations, the top layer is the most dynamically active as it is directly influenced by the external forcing and has the lowest inertia due to the smaller layer thickness. It clearly shows the emergence of zonal jets in the equatorial region, as is a common feature of geostrophic flows [46]. Away from the equator, no zonal jets form and the flow is qualitatively more isotropic. The lower two layers are indirectly forced by the upper layers. This forcing appears as a PV source term when the streamfunctions of two layers differ. Since the interaction term as seen in (27) contains a factor f^2, this source term is always smallest near the equator, which explains the low velocities in these regions after short simulation times as seen in the top row of Fig. 4. As the flow develops further, the internal dynamics of the lower layers result in a more homogeneous flow field.

While zonal jets form the dominant flow feature in the top layer, the lower layers show a more homogeneous distribution of kinetic energy in the flow domain. This is also clearly visible in the kinetic energy spectra of the layer-wise velocity fields shown in the left panel of Fig. 5. In blue, the kinetic energy spectrum of the top layer is shown in arbitrary units. The external forcing at $l = 50$ is visible in the spectrum, from which energy is distributed to all other modes. Furthermore, most energy is contained in harmonics with degree $l = 10 - 20$, which corresponds to the scale of the zonal jets. At high wavenumbers, the energy spectrum decays exponentially due to the eddy viscosity dissipation. The kinetic energy spectra of the lower layers exhibit largely the same structure as the top layer. However, the modes corresponding to the zonal jets have a significantly lower amplitude, indicating that zonal jets do not dominate the flow in these layers. In contrast, most kinetic energy in these layers is contained in the modes with degree $l = 20 - 30$, corresponding to structures with a size between 200 and 300 km, closely corresponding with the baroclinic Rossby radii. The numerical experiment has been repeated at resolutions $N = 512$ and $N = 256$. The obtained energy spectra of the top layer at $T = 2100$ are shown in the right panel of Fig. 5. We observe a good agreement in the distribution of energy across the resolvable scales at the different resolutions. This indicates that the previously discussed formation of zonal jets can be reproduced reliably also at lower resolution. This observation regarding the required level of spatial resolution was also made in relation to the corresponding single-layer QG model as presented previously in Cifani et al. [6], Franken et al. [7].

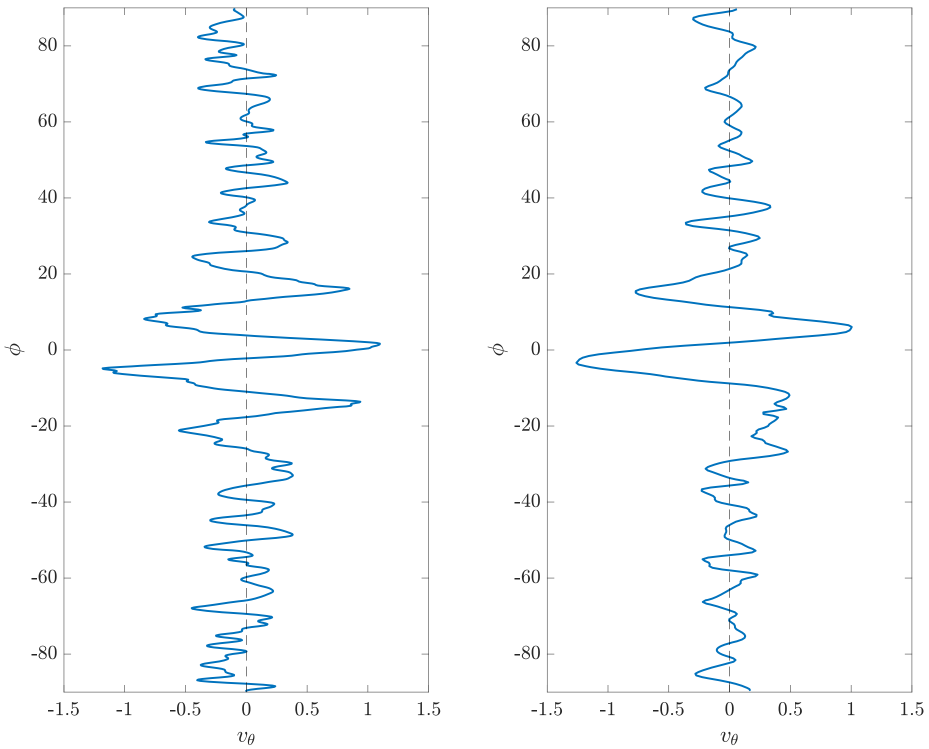

Fig. 7. Zonal velocity along a fixed longitude at time $T = 2100$ 'days', measured from the snapshots in 6. The left picture shows the zonal velocity in the top layer of a multi-layer simulation. The right picture shows the zonal velocity in single-layer QG turbulence with the same Rossby deformation radius.

In Fig. 6, a snapshot of the top layer zonal velocity field is compared to the simulation of single-layer barotropic QG dynamics with the same parameters as described above. The corresponding zonal velocity profiles along a fixed longitude are shown in Fig. 7. While geophysical interest would lie in prograde motion of the equatorial jet, it is difficult to discern a preferred direction of the flow relative to the 'Earth's' rotation. Furthermore, we observe that at high latitude the multi-layer prediction is similar to that of the single-layer model, while the multilayer model displays more variability near the equator compared to the classical single-layer QG model. Qualitatively, we find a striking similarity in the emergence of zonal jets. From previous studies [6,7], we infer that the Coriolis effect itself is enough to introduce alternating jets in rotating Euler and Navier-Stokes equations. The effect of the quasi-geostrophic approximation is to introduce a latitude-dependent zonal velocity modulation. One of the striking features that the QG model on the sphere is the transition from a region of alternating jets near the equator towards regions of more isotropic turbulence. The classical QG formulation based on a decomposition of the velocity field into geostrophic and ageostrophic components is known to break down near the equator. Here, we adopted the alternative solenoidal partitioning [11,12] which is known to alleviate the problems near the equator.

5. Conclusion and outlook

In this work, we presented a global formulation for the multilayer quasi-geostrophic (QG) equations and developed a Casimir-preserving numerical method for simulations. By extending the baroclinic QG models from traditional local f-plane or β-plane approximations to a global spherical framework, this work provides a comprehensive tool for studying large-scale atmospheric and global oceanic dynamics in the context of aqua-planets. To use the present model for simulations of more realistic ocean dynamics, continents have to be included, which at present is not yet possible.

The numerical method is based on similar global methods for the barotropic QG equations developed in Franken et al. [7], which in turn extends a study on the two-dimensional Euler equations in Cifani et al. [6]. In the current work, we developed a global formulation of the multilayer QG equation and applied a Casimir-preserving discretization to the resulting two-dimensional transport equations. This led to a finite-dimensional system which preserves all monomial Casimirs of the discrete system. Using a symplectic time integrator, we show that all discrete Casimirs are preserved up to a relative error of 10^{-8}.

The developed method was employed to simulate forced geostrophic turbulence. We have shown that zonal jets form at the top layer, which agrees with simulations on a single-layer model. Furthermore, we show from the kinetic energy spectra that the dynamics of the lower layers mostly concentrate near the respective baroclinic Rossby radii. The development of this novel numerical framework paves the way for application in large-scale simulations of global atmospheric and ocean dynamics. Further work is needed to develop benchmark simulations for geostrophic flow on a sphere and compare the proposed structure-preserving method to other computational methods.

The Zeitlin truncation is the only method known today that connects a continuous Poisson bracket into a discrete Poisson bracket. In [8] we established that pseudo-spectral methods perform well with regards to an inverse energy cascade, but do not perform well with regards to the forward enstrophy cascade even at high resolution. In contrast, the Zeitlin method performs well also in capturing the forward cascade at modest resolution. How this compares to a general finite-element method for simulation fluid flow on the sphere is a timely question that we will pursue in a separate study, clarifying when the full Zeitlin approach is warranted and when classical methods would be adequate.

While the model spheres considered in the manuscript apply conceptually to global atmospheric dynamics and aquaplanets, the oceanography of planet Earth is quite different and vastly more complex. Current extensions of the Zeitlin method are being pursued that will enable the inclusion of continents and explicit bathymetry. This will allow the application of the multilayer quasi-geostrophic model to oceanic QG formulations, thereby also providing further opportunities for direct validation of the predictions.

CRediT authorship contribution statement

Arnout D. Franken: Writing – review & editing, Writing – original draft, Visualization, Validation, Software, Methodology, Investigation, Formal analysis, Conceptualization; **Erwin Luesink:** Writing – review & editing, Validation, Methodology, Conceptualization; **Sagy R. Ephrati:** Writing – review & editing, Methodology, Conceptualization; **Bernard J. Geurts:** Writing – review & editing, Supervision, Project administration, Funding acquisition, Conceptualization.

Data availability

Data will be made available on request.

Declaration of competing interest

The authors declare that they have no known competing financial interests or personal relationships that could have appeared to influence the work reported in this paper.

Acknowledgements

The authors gratefully acknowledge the valuable discussions with Darryl Holm (Imperial College London) and Paolo Cifani. The authors would also like to thank the referees for their valuable comments and suggestions. This publication is part of the project SPRESTO which is financed by the Dutch Research Council (NWO) in their TOP1 program. EL was supported by NWO grant VI.Vidi.213.070. Simulations were carried out on the Dutch national e-infrastructure with the support of SURF Cooperative.

References

[1] P. Bechtold, N. Semane, S. Malardel, Convection and waves on small planets and the real Earth, in: Parameterization of Atmospheric Convection: Volume 2: Current Issues and New Theories, World Scientific, 2016, pp. 59–73.
[2] S. Chen, R.E. Ecke, G.L. Eyink, M. Rivera, M. Wan, Z. Xiao, Physical mechanism of the two-dimensional inverse energy cascade, Phys. Rev. Lett. 96 (8) (2006) 084502.
[3] Z. Xiao, M. Wan, S. Chen, G.L. Eyink, Physical mechanism of the inverse energy cascade of two-dimensional turbulence: a numerical investigation, J. Fluid Mech. 619 (2009) 1–44.
[4] I.V. Shevchenko, P.S. Berloff, Multi-layer quasi-geostrophic ocean dynamics in eddy-resolving regimes, Ocean Model. 94 (2015) 1–14.
[5] E. Hairer, C. Lubich, G. Wanner, Geometric numerical integration, 31 of *Springer Series in Computational Mathematics*, Springer-Verlag, Berlin, second ed., 2006. Structure-preserving algorithms for ordinary differential equations.
[6] P. Cifani, M. Viviani, K. Modin, An efficient geometric method for incompressible hydrodynamics on the sphere, J. Comput. Phys. 473 (2023) 111772.
[7] A.D. Franken, M. Caliaro, P. Cifani, B.J. Geurts, Zeitlin truncation of a shallow water quasi-geostrophic model for planetary flow, J. Adv. Model. Earth Syst. 16 (6) (2024) e2023MS003901.
[8] P. Cifani, M. Viviani, E. Luesink, K. Modin, B.J. Geurts, Casimir preserving spectrum of two-dimensional turbulence, Phys. Rev. Fluids 7 (8) (2022) L082601.
[9] G.K. Vallis, Atmospheric and Oceanic Fluid Dynamics, Cambridge University Press, 2017.
[10] J. Pedlosky, Geophysical Fluid Dynamics, Springer Science & Business Media, 2013.
[11] W.H. Schubert, R.K. Taft, L.G. Silvers, Shallow water quasi-geostrophic theory on the sphere, J. Adv. Model. Earth Syst. 1 (2) (2009).
[12] W.T.M. Verkley, A balanced approximation of the one-layer shallow-water equations on a sphere, J. Atmos. Sci. 66 (6) (2009) 1735–1748.
[13] N.A. Phillips, Geostrophic motion, Rev. Geophys. 1 (2) (1963) 123–176.
[14] R. Salmon, Baroclinic instability and geostrophic turbulence, Geophys. Astrophys. Fluid Dyn. 15 (1) (1980) 167–211.
[15] V. Zeitlin, Geophysical Fluid Dynamics: Understanding (Almost) Everything with Rotating Shallow Water Models, Oxford University Press, 2018.
[16] G.K. Vallis, Essentials of Atmospheric and Oceanic Dynamics, Cambridge University Press, 2019.
[17] D.D. Holm, J.E. Marsden, T. Ratiu, A. Weinstein, Nonlinear stability of fluid and plasma equilibria, Phys. Rep. 123 (1–2) (1985) 1–116.
[18] D.D. Holm, B. Long, Lyapunov stability of ideal stratified fluid equilibria in hydrostatic balance, Nonlinearity 2 (1) (1989) 23.
[19] E. Luesink, A. Franken, S. Ephrati, B. Geurts, Geometric derivation and structure-preserving simulation of quasi-geostrophy on the sphere, arXiv:2402.13707 (2024).
[20] E.N. Lorenz, Energy and numerical weather prediction, Tellus 12 (4) (1960) 364–373.
[21] R. Daley, Linear non-divergent mass-wind laws on the sphere, Tellus A 35 (1) (1983) 17–27.
[22] P. Ripa, Baroclinic instability in a reduced gravity, three-dimensional, quasi-geostrophic model, J. Fluid Mech. 403 (2000) 1–22.
[23] R. Salmon, Two-layer quasi-geostrophic turbulence in a simple special case, Geophys. Astrophys. Fluid Dyn. 10 (1) (1978) 25–52.
[24] E. Gkioulekas, The effect of asymmetric large-scale dissipation on energy and potential enstrophy injection in two-layer quasi-geostrophic turbulence, J. Fluid Mech. 694 (2012) 493–523.
[25] E. Luesink, Stochastic geometric mechanics of thermal ocean dynamics, Ph.D. thesis, Imperial College London, 2021.
[26] V. Zeitlin, Self-consistent finite-mode approximations for the hydrodynamics of an incompressible fluid on nonrotating and rotating spheres, Phys. Rev. Lett. 93 (26) (2004) 264501.
[27] L. Thiry, L. Li, G. Roullet, E. Mémin, MQGeometry-1.0: a multi-layer quasi-geostrophic solver on non-rectangular geometries, Geosci. Model Dev. 17 (4) (2024) 1749–1764.
[28] P. Cifani, S. Ephrati, M. Viviani, Sparse-stochastic model reduction for 2D Euler equations, in: Stochastic Transport in Upper Ocean Dynamics Annual Workshop, Springer Nature Switzerland Cham, 2022, pp. 17–28.
[29] V. Zeitlin, Finite-mode analogs of 2D ideal hydrodynamics: coadjoint orbits and local canonical structure, Physica D 49 (3) (1991) 353–362.
[30] M. Bordemann, J. Hoppe, P. Schaller, M. Schlichenmaier, gl(∞) and geometric quantization, Commun. Math. Phys. 138 (1991) 209–244.
[31] J. Hoppe, Diffeomorphism groups, quantization, and SU (∞), Int. J. Mod. Phys. A 4 (19) (1989) 5235–5248.
[32] J. Hoppe, S.-T. Yau, Some properties of matrix harmonics on S 2, Commun. Math. Phys. 195 (1998) 67–77.
[33] M. Bordemann, E. Meinrenken, M. Schlichenmaier, Toeplitz quantization of Kähler manifolds and gl(N), $N \to \infty$ limits, Commun. Math. Phys. 165 (1994) 281–296.
[34] K. Chen, Matrix Preconditioning Techniques and Applications, 19, Cambridge University Press, 2005.
[35] D.S. Watkins, Isospectral flows, SIAM Rev. 26 (3) (1984) 379–391.
[36] K. Modin, M. Viviani, A casimir preserving scheme for long-time simulation of spherical ideal hydrodynamics, J. Fluid Mech. 884 (2020) A22.
[37] K. Modin, M. Viviani, Lie–Poisson methods for isospectral flows, Found. Comput. Math. 20 (4) (2020) 889–921.
[38] M. Blackburn, B.J. Hoskins, Context and aims of the aqua-planet experiment, J. Meteorolog. Soc. Jpn. 91 (1) (2013) 1–15.
[39] S. Lee, Baroclinic multiple zonal jets on the sphere, J. Atmos. Sci. 62 (7) (2005) 2484–2498.
[40] J.-B. Gilet, M. Plu, G. Rivière, Nonlinear baroclinic dynamics of surface cyclones crossing a zonal jet, J. Atmos. Sci. 66 (10) (2009) 3021–3041.
[41] J. Chai, Understanding geostrophic turbulence in a hierarchy of models, Ph.D. thesis, Princeton University, 2016.
[42] V.B. Zalesny, Variational method for solving the quasi-geostrophic circulation problem in a two-layer ocean, Izvestiya, Atmos. Ocean. Phys. 58 (5) (2022) 423–432.
[43] G. Carigi, E. Luongo, Dissipation properties of transport noise in the two-layer quasi-geostrophic model, J. Math. Fluid Mech. 25 (2) (2023) 28.
[44] L. Li, B. Deremble, N. Lahaye, E. Mémin, Stochastic data-driven parameterization of unresolved eddy effects in a baroclinic quasi-geostrophic model, J. Adv. Model. Earth Syst. 15 (2) (2023) e2022MS003297.
[45] G. Boffetta, S. Musacchio, Evidence for the double cascade scenario in two-dimensional turbulence, Phys. Rev. E 82 (1) (2010) 016307.
[46] R.K. Scott, D.G. Dritschel, The structure of zonal jets in geostrophic turbulence, J. Fluid Mech. 711 (2012) 576–598.